6

8

9

10

11

12

13

14

15

17

18

19

20

21

22

23

24

25

26

27

28

30

31 32

33

34 35

Finger Force Estimation Using Motor Unit Discharges Across Forearm Postures

Noah Rubin, Yang Zheng , He Huang, and Xiaogang Hu

Abstract-Background: Myoelectric- based decoding has gained popularity in upper- limb neural-machine interfaces. Motor unit (MU) firings decomposed from surface electromyographic (EMG) signals can represent motor intent, but EMG properties at different arm configurations can change due to electrode shift and differing neuromuscular states. This study investigated whether isometric fingertip force estimation using MU firings is robust to forearm rotations from a neutral to either a fully pronated or supinated posture. Methods: We extracted MU information from high- density EMG of the extensor digitorum communis in two ways: (1) Decomposed EMG in all three postures (MU-AllPost); and (2) Decomposed EMG in neutral posture (MU-Neu), and extracted MUs (separation matrix) were applied to other postures. Populational MU firing frequency estimated forces scaled to subjects' maximum voluntary contraction (MVC) using a regression analysis. The results were compared with the conventional EMG-amplitude method. Results: We found largely similar root-mean-square errors (RMSE) for the two MU-methods, indicating that MU decomposition was robust to postural differences. MU-methods demonstrated lower RMSE in the ring (EMG = 6.23, MU-AllPost = 5.72, MU-Neu = 5.64%MVC) and pinky (EMG = 6.12, MU-AllPost = 4.95, MU-Neu = 5.36% MVC) fingers, with mixed results in the middle finger (EMG = 5.47, MU-AllPost = 5.52, MU-Neu = 6.19% MVC).Conclusion: Our results suggest that MU firings can be extracted reliably with little influence from forearm posture, highlighting its potential as an alternative decoding scheme for robust and continuous control of assistive devices.

Index Terms—Biosignal processing, Finger force estimation, Forearm posture, Motor unit decomposition, Neural decoding.

Manuscript received September 6, 2021; revised December 6, 2021 and January 29, 2022; accepted February 19, 2022. This work was supported by the National Science Foundation under Grants IIS-1954587, CBET-1847319, and IIS-2106747. (Corresponding author: Xiaogang Hu.)

Noah Rubin and He Huang are with the Joint Department of Biomedical Engineering, University of North Carolina-Chapel Hill, USA, and also with the North Carolina State University, USA.

Xiaogang Hu is with the Joint Department of Biomedical Engineering, University of North Carolina-Chapel Hill, Chapel Hill, NC 27599 USA, and also with the North Carolina State University, Raleigh, NC 27695 USA (e-mail: xiaogang@unc.edu).

Yang Zheng is with the Institute of Engineering and Medicine Interdisciplinary Studies, School of Mechanical Engineering, Xi'an Jiaotong University, China.

This article has supplementary downloadable material available at https://doi.org/10.1109/TBME.2022.3153448, provided by the authors. Digital Object Identifier 10.1109/TBME.2022.3153448

I. INTRODUCTION

37

38

40

44

46

48

49

50

51

52

53

54

55

59

61

65

66

67

68

69

70

71

73

74

75

76

77

78

80

N RECENT decades, neural-machine interfaces have advanced with promise to assist and rehabilitate individuals with motor impairments by decoding user intent to control assistive devices [1]. Different techniques have been developed to record activity at varying levels of the nervous system. Electroencephalography [2], electrocorticography [3], and intracortical arrays [4] allow brain- machine interfaces, while peripheral nerve implants [5] and surface electromyography (EMG) [6] enable communication from the peripheral nervous system. The EMG signal reflects the summation [7] of motor unit action potentials (MUAPs) from a number of motor units (MUs) (each a motor neuron and all the muscle fibers it innervates), considered the smallest independent control units of muscle activation [8]. The EMG- amplitude signal gives a global measure of activation, and historically has been employed widely in myoelectric control of assistive robots in the upper limb [9], [10], as it provides a noninvasive, easy-to-implement input signal.

Current state-of-the-art commercial devices frequently use time/frequency features of EMG to classify user intent into discrete gestures via pattern recognition [11]–[13]. Further efforts have combined gestures for simultaneous actuation [14], but this relates control of independent degrees of freedom, constraining the available workspace. Additionally, as design of assistive robotic hands continues advancing with multi-finger control to mimic a biological hand, maintaining high classification accuracies becomes challenging. Alternatively, continuous decoding schemes may allow more dexterous control than pattern recognition. Recent studies have employed neural network-[15], [16], regression- [17], and physiologically- based models [18], [19] to enable continuous and simultaneous control. Concurrently, blind source separation techniques have been developed to decompose EMG into individual MU firing activities [20]–[24]. Populational MU firing frequency has been demonstrated as an accurate continuous control input signal to approximate motor output via neural drive [25] using the firing frequency of the summation of firing events of multiple MUs [26].

All the above-mentioned decoding schemes rely on EMG signals. However, EMG signals easily degrade due to multiple factors, such as background noise [27], motion artifacts [28], and crosstalk between adjacent muscles [29]. In addition, EMG properties can vary substantially at different arm configurations. For example, electrode shift of 1 cm relative to skin [30] and across forearm orientations [31] can significantly increase pattern classification error. Furthermore, voluntary activation

[32] and capacity of force generation [33] can vary with arm posture, imposing interference to motor intent decoding. Using populational MU firing frequency, it is currently unclear how well fingertip force prediction generalizes to multiple forearm postures. Across the range of forearm rotational postures, the electrode-muscle interface may change the MUAPs significantly, making it difficult to accurately identify MUAP trains consistently. As the field progresses towards control in more realistic settings, it is necessary to test whether MU decomposition is robust to postural effects on EMG signals. In our study, we asked two primary questions:

- 1) Is force prediction via populational MU firings robust to arm postural effect?
- 2) Does populational MU firing frequency outperform EMG-amplitude in force prediction of isometric finger extension across the forearm's range of rotational motion?

Specifically, we asked able-bodied subjects to produce isolated isometric finger extension while their forearm was maintained in three different postures: fully pronated, neutral, and fully supinated, spanning its range of motion. We first quantified the shift of spatial activation patterns of the finger extensor muscles at these forearm postures using high- density EMG activation maps. We then compared force prediction performance of MU- and EMG-based methods in all postures. To test the robustness of MU decomposition to postural effect, we extracted MU activities in real-time in two methods: First, MU decomposition was performed only in the neutral posture using an independent component analysis (ICA) algorithm [34], and extracted MU information (i.e., separation matrix) was applied directly to EMG obtained in the other two postures (MU-Neu). Second, MUs were decomposed from EMG in all postures (MU- AllPost). We then calculated the populational MU firing frequency of each MU method and employed regression analysis to estimate individual fingertip forces. As a comparison, we used EMG-amplitude, after a channel-refinement procedure to remove cross-talk, to estimate individual fingertip forces. Our results suggest MU decomposition is robust to postural effects on electrode shift, muscular states, and neural activation. Overall, the outcomes from this study further highlight the potential of MU decomposition as an alternative neural decoding scheme for continuous control of assistive robotic hands.

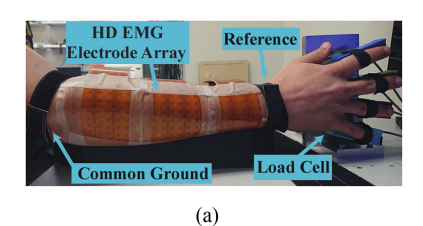
II. METHODS

A. Subject Recruitment

Seven healthy subjects (5 males, 2 females, 20-35 years of age) without any history of neurological or muscular disorders participated in this study. All provided informed consent of protocols approved by the local Institutional Review Board.

B. Data Acquisition

Each subject was seated in an adjustable experimental chair with their right forearm resting on a foam pad. Their right wrist was secured between two padded boards attached to the table and overlaid with Velcro straps for fixation. Each finger was fixed to 3D-printed attachments against a load cell measuring



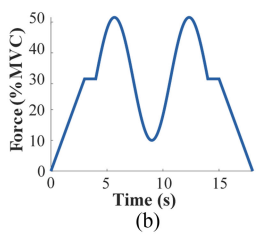


Fig. 1. Experimental Setup. (a) High- density EMG arrays were placed along the extensor digitorum communis. Reference and common ground electrode straps were placed on the wrist and elbow, respectively, with each finger strapped to a load cell measuring finger force outputs. Load cells were attached to a support system that rotated the wrist between a fully pronated, neutral, and fully supinated postures. Only the neutral posture is shown as an example. (b) One repetition (7 total per trial) of the force trajectory provided via visual feedback.

force output (SM- 200N, Interface, Scottsdale, AZ, 1 kHz). Additional Velcro straps fixed fingers to the load cells for accurate measurement of isometric extension forces (Fig. 1(a)). Supports connecting the load cell to the table allowed for modular rotation of the forearm into all postures tested.

Two or three 8x8 electrode arrays (128-192 channels) of high-density EMG electrodes with a 10 mm inter-electrode distance and 3 mm electrode diameter (OT Bioelettronica, Torino, Italy) was used to record EMG (Fig. 1(a)) and accommodate different forearm sizes. The EMG pads were adhered along the extensor digitorum communis while the subject's wrist rested at neutral. This muscle was chosen due to its superficial location for reasonable signal quality and involvement in multiple digit actuation in finger extension, a vital functionality for dexterous object manipulation. EMG data were acquired via monopolar channel recording with a reference electrode on the wrist and common ground at the elbow. Data were sampled with a gain of 1000 and filtered between 10-900 Hz via the EMG- USB2 + system (OT Bioelettronica, Torino, Italy, 2048 Hz).

The experiment was conducted in three blocks corresponding to three postures (random order). Within each posture, the index, middle, ring, and pinky fingers were tested in separate trials, giving twelve trials in total (3 postures × 4 fingers). Before each set of trials in a posture, subjects first conducted their maximum voluntary contraction (MVC) for each finger in a random order. Then in the same order, for each finger, subjects followed a force trajectory varying from 0-50% MVC for a duration of 18-seconds (Fig. 1(b)) that repeated 7 times to maximize the pool of recruited MUs, with 5-seconds of rest between repetitions. This force trajectory was chosen to test each model's ability to modulate with dynamic states of neural activation, as would be observed in real- world activities. 30-seconds of rest was provided between different finger trials within a posture, and 5-minutes of rest between different posture blocks.

C. Data Processing

1) EMG Channel Selection: All analysis described below was conducted for each finger independently. To adequately capture relevant muscle activity across postures for channel selection, an automated procedure removed signal interference [35] from the EMG signals (see Fig. S2 for examples), the

root-mean-square (RMS) for each EMG channel within an entire trial was calculated, and the RMS across the three trials from each posture was averaged. Informed visual inspection was used to remove any dead channels, as conducted in [36] (up to 10 for each subject, often at the edge of an array due to poor contact, as seen in Figure S1 as an example). Thereafter only the 85 channels with the highest average RMS were used for further analysis. We chose 85 as a reasonable value based on prior work that showed compartmentalization of individual finger activation [37], and success in force and joint angle prediction in one forearm posture with a static selection of 64 channels [38], [39]. Because a prior simulation study on forearm flexor muscle activation showed no significant difference in MU decomposition accuracy between using 44, 54, and 64 channels [40], we increased the channel threshold from 64 to 85 to account for a potentially larger distribution of muscle activity across all postures in preliminary observations.

2) Comparing Muscle Activity Between Conditions: To quantify the distribution of muscle activity and compare between postures and fingers, for each trial, the geometric centroid of the muscle activity was calculated (1). While different distributions may result in the same centroid location, we used this metric because the distribution did not drastically change across postures (Fig. 3). The x & y axes were defined along the medial-lateral and proximal-distal directions along the pads, respectively, with the origin at the most medial and proximal channel. As conducted in [37], [41], we computed the centroid coordinates for each axis C_x and C_y as follows:

$$C_x = \frac{\sum_{i=1}^{85} C_{ix} RMS_i}{\sum_{i=1}^{85} RMS_i}, C_y = \frac{\sum_{i=1}^{85} C_{iy} RMS_i}{\sum_{i=1}^{85} RMS_i}$$
(1)

where C_{ix} and C_{iy} are the i^{th} channel's geometric location (in mm) from the respective medial-lateral and proximal-distal axes origins, and RMS_i is the root-mean-square voltage of the i^{th} channel.

The magnitude of the Euclidean distance between the pronated and neutral centroids and the neutral and supinated centroids were calculated, and no significant differences were observed (using a paired t-test, after checking for normality via the Shapiro-Wilk test [42], $p=0.51,\,0.35,\,0.54,\,0.79$ for the index, middle, ring, and pinky fingers respectively). To summarize shifts in activity across the forearm's rotational range of motion, these magnitudes were summed.

3) Force Prediction:

a) Data Segmentation: EMG data from the first repetition within every trial (EMGi) was exclusively used for the initial offline MU decomposition (see Supplementary Materials for details). The MU- AllPost method included independent decompositions of EMGi in the neutral, pronated, and supinated postures, resulting in three sets of separation vectors w_n , w_p , and w_s , respectively. Thereafter, unique MUs from w_n , w_p , and w_s were retained. Alternatively, the MU-Neu method decomposed MUs from EMG_i only in the neutral posture (Fig. 2(a)), and the separation vectors were directly applied to EMG_i in the other two postures. For regression model training/testing, the remaining 6 repetitions in a trial were split and concatenated with corresponding repetition numbers from trials for each posture.

This gave six data blocks, each including EMG and force data from all postures. A 6-fold cross-validation was then performed (five training, one testing) to evaluate models' performances. By comparing the MU-AllPost and MU-Neu methods, we determined whether MUs decomposed from EMG of a single posture could perform equivalently to those decomposed in each posture when estimating force output in all postures.

b) Force Estimation Using Neural Drive: Force data was low-pass filtered (4th order Butterworth [43], 2 Hz cutoff) and normalized to each trial's respective MVC for estimation. To mimic an environment suitable to later implement controller updates during a real-time acquisition, an online analysis was conducted, where EMG was band-pass filtered 5-500 Hz [43], extended, and whitened in 1-second increments, as conducted in [44]. Separation vectors w of remaining MUs after offline decomposition were then applied to each increment to gather respective source signals, and MU spike trains were extracted (Fig. 2(b)) [44]. There is potential recruitment of MUs activating non-targeted fingers or inclusion of unreliable source signals for force prediction. Rather than using all remaining active MUs for the final trained model, we conducted a refinement procedure to improve force estimation for the targeted finger, (Fig. 2(c)): firing rates (FRs) of individual MUs (0.5-second window, 0.1second step size as done in [45]) were calculated, smoothed with a Kalman filter [46], and linearly regressed to the corresponding finger's force level, because the firing frequency associated with a particular finger should correlate with its motor output. Up to 10 MUs with the highest coefficients of determination (R²) were kept. The cumulative spike train of 10 MUs is sufficient to represent the common synaptic input to motor neurons, an indirect measure of effective neural drive [47], and prevents inclusion of MUs with poor force estimation performance. The final trained model fit refined MU FRs to force via multiple linear regression as follows:

$$F(t) = \sum_{j} a_{j} F R_{j}(t) + b$$
 (2)

where F(t) and $FR_j(t)$ are respectively the force and smoothed FR of the *j*th MU at time t, a_j is the *j*th MU's fit coefficient, and b is the fit y-intercept.

Separation vectors of the refined MUs were then applied to identically processed EMG in the test set; spike trains were extracted, and smoothed FRs were input into the trained model to estimate force. Negative estimates of force were set to zero; while it is possible flexors were active at higher forces, we only recorded finger extensors during the task.

c) Force Estimation Using EMG-Amplitude: EMG training sets were filtered and channel refinements were also performed to only include channels recording isolated activation of the targeted finger. The same moving window (0.5-second, 0.1-second step size) computed the RMS of EMG and an identical Kalman filter [46] as in the neural drive calculation smoothed the computed result. The smoothed RMS of each channel was then linearly regressed to force from the entire training set. To control comparisons between the EMG-and MU-based methods, the 10 channels with the highest R² values were kept. The average smoothed RMS of these channels was linearly regressed to force to create a trained model to predict force across all

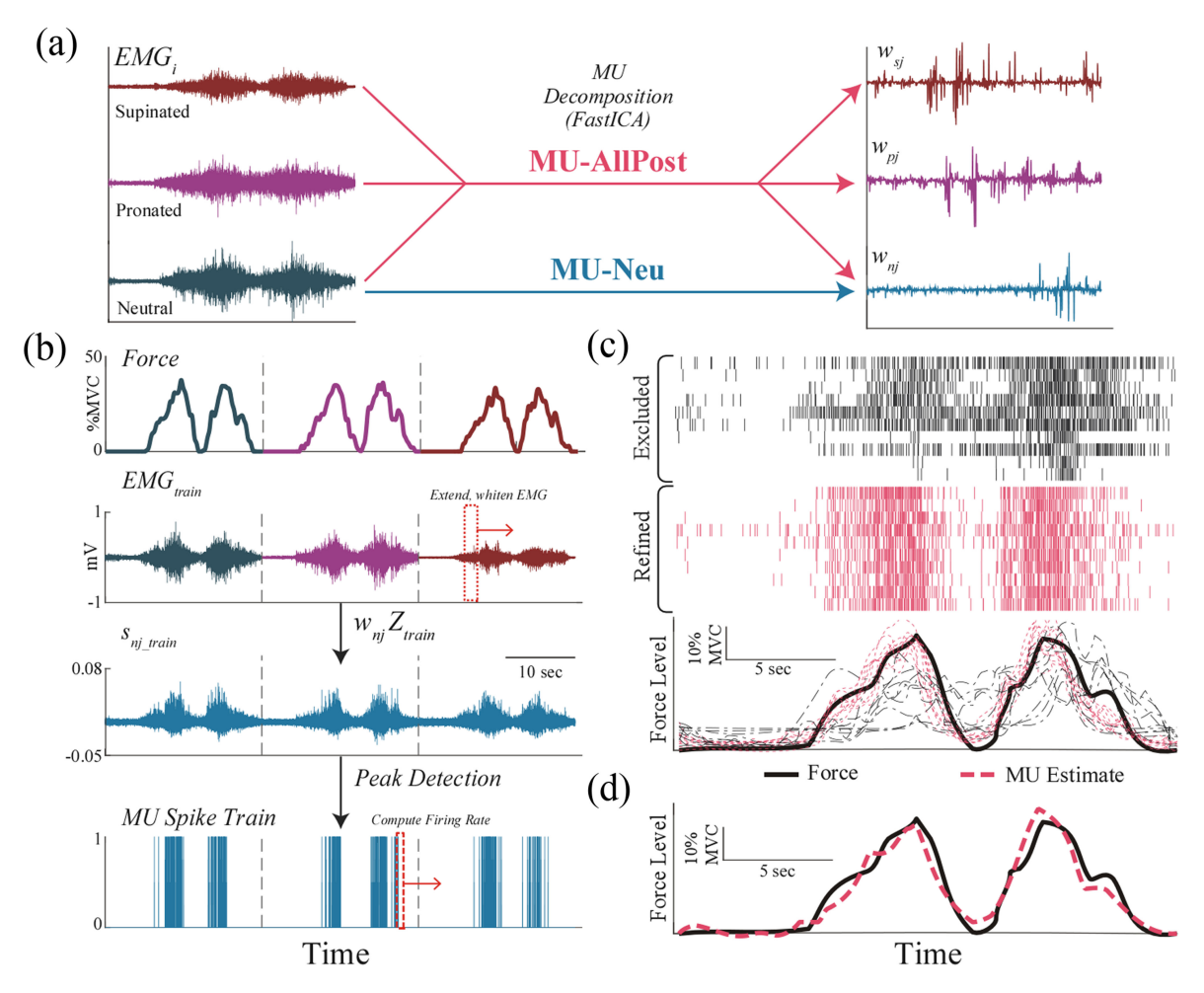


Fig. 2. Training MU Force Estimation Model. (a) EMG in the first repetition of a trial (EMG_i) in neutral, pronated, and supinated postures were each decomposed offline (see Supplementary Materials) into sets of separation vectors \mathbf{w}_n , \mathbf{w}_p , \mathbf{w}_s , respectively. Each vector in the set corresponds to a given jth MU. The MU- AllPost method used \mathbf{w}_n , \mathbf{w}_p , \mathbf{w}_s , while the MU- Neu method only used \mathbf{w}_n in force estimation. (b) After offline decomposition, in the training set (for brevity one of five data blocks is shown), separation vectors (in this case, \mathbf{w}_{nj}) were applied online using a moving window (red dashed box) extended and whitened EMG, $\mathbf{Z}_{\text{train}}$, unmixing MU information into a source signal \mathbf{s}_{j} -train. Peak detection via K-means clustering converted this signal into a MU spike train, and a moving window across each spike train calculated MU FRs. (c) Representative spike trains of excluded (black) and refined (red) MUs. Individual MU FRs (thin dashed lines) were linearly regressed to force (solid black line). The 10 MUs with the highest R² values (red, Refined set) were kept. (d) Refined MU FRs were used in multiple linear regression to force, giving the trained model estimation (thick dashed line). For visual brevity, one repetition from a single posture in the training set is displayed.

postures. The 10 refined channels were identically processed in EMG from the test set and input into the trained model to estimate finger force. Negative estimates of force were again set to zero. The root-mean- square error (RMSE) between predicted and actual force levels of the test set was calculated to evaluate model performance.

4) Statistical and Residual Analysis: A significance threshold of $\alpha=0.05$ was used for all statistical tests, and all data were first checked for normality (Shapiro-Wilk test [42]) prior to conducting parametric tests. For each finger, a paired t-test compared EMG activity shifts between postures (i.e., the shift magnitude from neutral to pronated and neutral to supinated postures). To compare shifts between fingers, a one- way analysis of variance (ANOVA) tested for significant differences in the summed magnitudes across postures. Performances between the EMG, MU- AllPost, and MU- Neu methods were analyzed for each finger independently. Data were tested

for sphericity (Mauchly's test [48]), and a repeated measures ANOVA between methods determined significant differences. If significant differences were observed above, multiple pairwise comparisons with a Bonferroni correction were conducted. In addition to statistical analysis of overall RMSE, residual analysis of the regression was conducted to quantify performance across force levels (see supplementary material for details).

III. RESULTS

A. Muscle Activity Across Postures

To illustrate muscle activity in each trial, Fig. 3 shows representative heat maps across trials for subject 1, overlaid with the geometric centroid of muscle activation. The index finger had two distinct areas of activation distally and slightly proximally relative to the midline of the pads. Prior work has shown one distinct peak of activation during isolated index finger extension

360

361

362

363

364

365

366

367

368

369

370

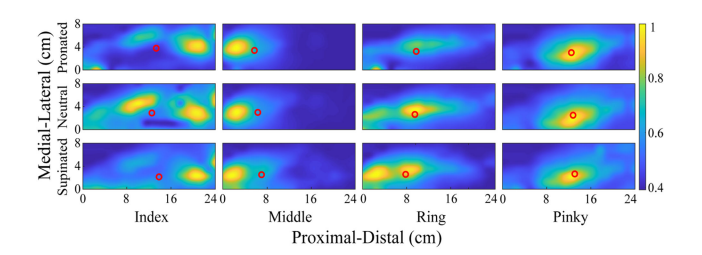


Fig. 3. Representative heat maps (subject 1) of muscle activation across each finger and posture. Muscle activation was normalized to the EMG channel with the highest RMS within each trial. The overlaid red circles indicate the geometric centroid of muscle activation.

316

317

318

319

320

321 322

323

324

325 326

327

328

329

330

331

332

333

334

335

336

337

338

339

340

341

342

343

344

345

346

347

348

349

350

351

352

353

354

355

356

357

358

[37], [49], [50], suggesting subjects may have had more coactivation with other fingers in this study. Markedly, the middle finger had concentrated activation in the most proximal region. The ring and pinky fingers had the highest activity slightly proximally and centrally with wide distributed activity across the pads. While activation regions for each finger were consistent across subjects, the relative shift in the centroid between postures varied (Fig. S3). For each finger in the medial-lateral direction, across the range of motion (i.e., from pronated to a neutral and neutral to a supinated posture) the centroid shifted in the same direction for 3-4 subjects, while the direction switched at the neutral posture for others. More specifically, subjects 1 and 5's centroids shifted medially across the range of motion in all fingers except for neutral to supinated in the pinky and pronated to neutral in the middle finger, respectively. Opposing this, subject 4 and 6's centroid shifted laterally and then medially, except for pronated to neutral for the index finger of subject 6. In contrast, subject 2's centroid always shifted medially from pronated to neutral and then the direction switched laterally from neutral to supinated. Subjects 3 and 7 exhibited more varied medial-lateral shifts across all conditions. In the proximal-distal direction, shifts were more consistent across subjects, but still differed across fingers. Index finger activity shifted proximally for all but subject 6 from pronated to neutral and subjects 3-6 from neutral to supinated. In the middle finger, activity in all but subject 3 shifted distally from pronated to neutral, with more variation when moving to a supinated posture. The ring finger consistently had proximal shifts across the range of motion, except for subjects 6-7 moving to neutral and 4 moving to supinated. In the pinky, subjects 1, 2, 4, and 6 shifted the same direction across the range of motion, but in this case there was variation in which direction across subjects.

Resulting data on shifts in muscle activity were found to have a normal distribution. Even though there was large variation in the direction of shift for the muscle activation centroids across the range of motion, no significant differences in the magnitude of shifts from a neutral to either pronated or supinated postures were observed (p = 0.36, 0.95, 0.59, 0.67 for the index, middle, ring, and pinky fingers respectively). Thus, we summed the centroid shift magnitude across the range of motion to summarize changes in the activity distribution (Fig. 4). The index finger had the largest mean magnitude shift across subjects (2.66 \pm 0.93 cm), followed by the ring (2.24 \pm 1.00 cm), pinky (1.42 \pm

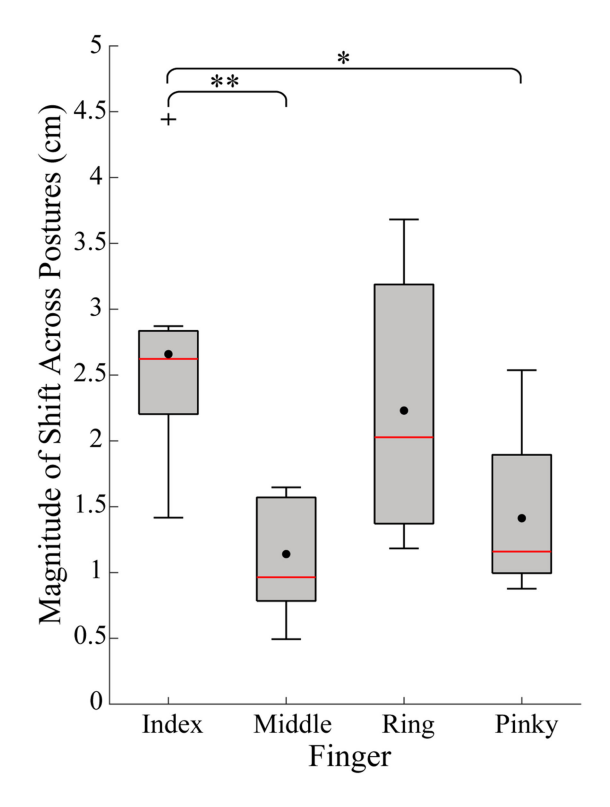


Fig. 4. Boxplot of the magnitude of Euclidean shift in the muscle activity's geometric centroid across the range of motion (pronated to neutral to supinated) for all subjects. Overlaid black dots indicate sample means (*p < 0.05, ** p < 0.01).

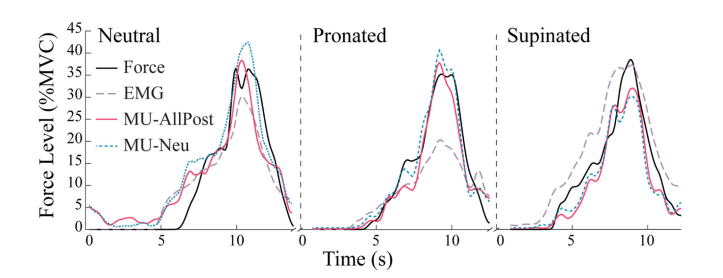


Fig. 5. Force estimation evaluation. After model training, refined MUs' firings and refined EMG channels' RMS activity were employed to predict force across all postures in the test set (subject 2, ring finger displayed as representative example). For visual brevity, half of the test set is shown.

0.65 cm), and middle fingers (1.11 \pm 0.45 cm). The index finger had a significantly greater shift magnitude than the middle (p = 0.006) and pinky (p = 0.032) fingers.

B. Force Prediction Performance

Fig. 5 shows representative force predictions for the EMGand MU-based methods in a test set from subject 2's ring finger. Note the same refined EMG channels and MUs were used when testing across all postures. The EMG-amplitude method (dashed, purple line) underestimated force at high effort levels (black line) in the neutral and pronated postures. The MU- Neu (red line) and MU- AllPost (dashed, green line) methods outperformed the EMG method at mid-range force levels (10-30% MVC), and

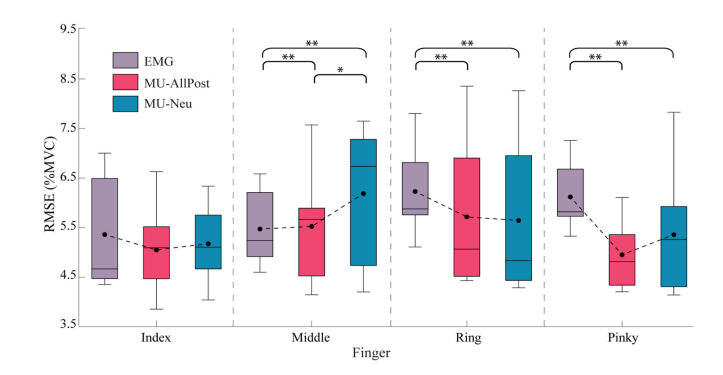


Fig. 6. Estimation error across fingers for each method. The distribution across subjects is shown (boxplot) and overlaid with the average error (black dot) in test sets (*p < 0.01, **p < 0.0001).

TABLE I STATISTICAL COMPARISONS BETWEEN METHODS

| | Finger | | | |
|---------------|--------|----------|----------|----------|
| | Index | Middle | Ring | Pinky |
| All Methods | 0.12 | < 0.05 | < 0.05 | < 0.0001 |
| | (2.37) | (6.48) | (5.61) | (26.8) |
| EMG vs | | < 0.0001 | < 0.0001 | < 0.0001 |
| MU-AllPost | | | | |
| EMG vs | | < 0.0001 | < 0.0001 | < 0.0001 |
| MU-Neu | | | | |
| MU-AllPost vs | | < 0.01 | > 0.99 | 0.10 |
| MU-Neu | | | | |

Bold values indicate statistically significant differences.

 $\alpha = 0.05$ and the critical F-statistic is 3.23

371

372

373

374

375

376

377

378

379

380

381

382

383

384

385

386

387

388

389

390

391

392

393

394

395

396

397

398

quickly adjusted to changes in force. Both EMG-and MU-based methods had varied performance at zero force across postures, with better performance in pronated and supinated postures compared to neutral in this case. Notably, except for peak forces in neutral, the MU-Neu and MU-AllPost methods had similar trajectories throughout the exemplar trial. For all three methods employed, regression tended to overestimate low forces and underestimate high forces produced (see Supplementary Materials), resulting in a slight proportional bias. Markedly, however, MU- based methods possessed less severe bias than the EMG method, and the MU-AllPost and MU-Neu methods maintained similar trends in prediction across force levels.

To summarize model performances, Fig. 6 shows the RMSE of each method across fingers averaged across subjects, and Table I summarizes statistical comparisons. Performance across methods were found to be normally distributed with sphericity. No significant differences were observed in RMSE between methods in the index finger ($\bar{x}_{EMG} = 5.36$, $\bar{x}_{MU-AllPost} =$ 5.05, $\bar{x}_{MU-Neu} = 5.18\%$ MVC). In all other fingers, significant differences in performance occurred between the EMG and both MU- based methods. The MU-based methods were significantly worse in the middle finger ($\bar{x}_{EMG} = 5.47$, $\bar{x}_{MU-AllPost} =$ 5.52, $\bar{x}_{MU-Neu} = 6.19\% \text{MVC}$), but with only a 0.05% RMSE difference in sample means between the EMG and MU- AllPost method. Notably, MU- based methods performed significantly better than the EMG- amplitude method in both the ring (\bar{x}_{EMG} $= 6.23, \bar{x}_{MU-AllPost} = 5.72, \bar{x}_{MU-Neu} = 5.64\% \text{MVC}$) and pinky ($\bar{x}_{EMG}=6.12,\ \bar{x}_{MU-AllPost}=4.95,\ \bar{x}_{MU-Neu}=$

5.36%MVC) fingers, but no significant difference was observed between the MU- based methods in either finger.

399

400

401

402

403

404

405

406

407

408

409

410

411

412

413

414

415

416

417

418

419

420

421

422

424

425

426

427

428

429

430

431

433

434

435

436

437

438

439

440

441

442

443

444

445

446

447

448

449

450

451

452

453

Performances for each subject are depicted in Fig. S5. Across most conditions, both EMG- and MU-based methods had RMSE values ranging from 4-10%. In the index finger, all methods had similar performance in subjects 2 and 4-7, with slightly better performance in EMG for subject 3 and slightly worse only for subject 1. All methods in the middle finger had varied performance across subjects. Unexpectedly, EMG outperformed MU- based methods in subjects 2, 4, and 6. However, both MU- based methods outperformed EMG in subjects 3 and 7, while in subjects 1 and 5 the MU- AllPost method outperformed EMG. In the ring finger, MU- based methods outperformed EMG in 5 subjects, with similar performance in subject 1 and slightly worse performance in subject 5. In the pinky, MU-based methods consistently outperformed EMG- amplitude methods in all subjects except for similar performance to the MU-Neu method in subject 2. Most notably, in the index, ring, and pinky fingers no significant differences were observed between the MU-Neu and MU-AllPost methods (Table I), but unexpectedly significant differences were observed in the middle finger (p < 0.01). Upon further inspection, individually only subjects 1 and 5 displayed significant differences (paired t-tests on the 6-folds, α = 0.05), whereas similar performance in the MU-based methods was seen in the other five subjects (Fig. S5).

IV. DISCUSSION

This study compared force estimation accuracy using conventional EMG-amplitude and MU discharges decomposed from high-density EMG of finger extensors at different forearm rotational angles spanning the range of motion. Our results revealed MU firing information (separation matrix) obtained in one position can be used to reliably extract MU information at different postures, as indicated by similar performance between the two MU methods. For most subjects and two of four fingers, MU methods outperformed (and if not, performed similarly with few exceptions) EMG-amplitude predicting isometric finger extension force across the range of a forearm's rotational angle. These outcomes further support use of MU discharges as an alternative input signal for assistive device control.

Across subjects, we observed varied results in the middle, similar performance in the index, and better performance with MUs in the ring and pinky fingers. Unexpectedly, the EMG-amplitude method outperformed MUs in 3 subjects for the middle finger. One potential explanation for these higher performances of the EMG-amplitude method is the isolation of the middle relative to other fingers. Earlier studies have led the hypothesis that finger muscles are compartmentalized into subunits [51], [52], and in a prior analysis involving high-density EMG during finger extension, the middle finger had the most distinct region of activation when compared to concurrent activation of all fingers [37]. This coincides with our study, as the spatial distribution of activation of the middle finger was most proximal and localized relative to other fingers (Fig. 3). Furthermore, the centroid of the muscle activation did not change substantially across all three postural conditions relative to other fingers (Fig. 4, S1).

455

456

457

458

459

460

461

462 463

464

465

466

467

468

469

470

471

472

473

474

475

476

477

478

479

480

481

482

483

484

485

486

487

488

489

490

491 492

493

494

495

496

497

498

499

500

501

502

503

504

505

506

507

508

509

510

511

512

513

515

516

517

518

519

520

521

522

523

524

525

526

527

528

530

531

532

533

534

535

536

538

539

540

541

542

543

544

545

546

547

548

549

550

551

552

553

554

555

557

558

559

560

562

563

In tandem with a localized region of activation, another study quantifying crosstalk between EMG recorded during individual finger extension observed the least amount of crosstalk during middle finger activation compared to other fingers [53]. Given the concentrated, isolated activation for this finger, refined channels were likely well-isolated to the middle finger compartment in all postures, which could afford a robust prediction with EMG-amplitude compared to other fingers. In less controlled settings involving simultaneous finger actuations, recorded EMG may not be as well-isolated, potentially degrading performance of the EMG method.

In the index finger, no significant difference between the EMG, MU-AllPost, and MU-Neu methods were observed. While not as isolated as the middle finger, the index finger also recruits less non-targeted fingers in voluntary single-digit activation [54]. Relative to other fingers, we observed a larger activation distribution across the pad and notably a higher centroid shift magnitude across postures (Fig. 4). While prior work has shown improved performance compared to traditional EMG in this finger in single postures [55], it is possible the neural strategy for muscle activation across postures differed, and thus different MUs were recruited at these positions, degrading the correlation of refined MUs for all postures and leading to comparable performance between the methods. However, for the ring and pinky fingers, the MU-based methods outperformed the EMG method for most subjects. Correspondingly, recent work predicting force with sequential activation of multiple fingers also showed the largest improvement in performance with MU-based compared to EMG-amplitude methods in the ring and pinky fingers activating concurrently [25]. Unlike the index and middle fingers, the muscle compartments of the ring and pinky are not as anatomically separated [56]. Hence, we observed similar regions of activation during these trials across postures compared to other fingers (Fig. 3). Additionally, greater enslavement (co-activation of non-targeted fingers) in these fingers has been documented [54], [57], [58]. Indeed, during our experiment subjects consistently reported having difficulty isolating these fingers. Even though the territory of a MU (region of innervated muscle fibers) is frequently localized [59], relating individual MUs to activation of individual fingers, the neural drive to MUs for isometric finger extension is often not well-isolated. There is often short-term synchronization [60] and high levels of common synaptic input to MUs between muscle compartments in the delta band [61], which is hypothesized to correlate with force modulation [26]. Furthermore, in individual finger extension, spillover of MU recruitment to non-targeted fingers occurs, with greater force production in the ring and pinky compared to the index and middle fingers [62], [63]. Therefore, since the ring and pinky compartments have less independent neural drive and close anatomical proximity, refined channels likely contained activity related to different fingers' force production. Instead, by conducting our refinement procedure to predict force at the MU-level, we better isolated activation related to force for a single digit. Hence, while EMG outperformed MUs only in a few cases for the most isolated (middle) finger, MUs outperformed EMG in the least isolated trials. In contexts requiring dexterous finger manipulation across multiple arm configurations, the potential for MUs to outperform EMG as a continuous control input signal may become more pronounced.

We also tested whether MU decomposition is robust to different arm postures by using MUs decomposed from EMG recorded only in the neutral posture (MU-Neu) to predict force output across all postures, and we compared this to using MUs decomposed from EMG recorded in all postures (MU-AllPost). Impressively, in most fingers and subjects the MU methods performed similarly. Given the consistent source signal across postures (Fig. 2B) and modulation of force prediction for the MU-Neu method in all conditions (Fig. 5), separation vectors from MU-Neu could identify MUs from EMG recorded in other postures, which can sufficiently represent neural drive to the muscle [47]. In future studies involving multiple arm postures, initial decomposition may only be needed from one position.

This study revealed MU decomposition of individual finger extensors is robust to forearm rotation, providing a novel application in force prediction. However, the investigation was limited in certain aspects. Subject-specific channel selection may improve computational efficiency or performance in translation to real-time control settings. Data were also constrained to a specific periodic trajectory. More variation between trained and tested models are needed to ensure robustness across all conditions of force prediction. More advanced refinement in the MU-based models could also be employed by adding weight to the most reliable MUs that are consistently better predictors of the control goal. Tests were also conducted at discretized states in isometric conditions. Prior work has decomposed MUs for myoelectric control with both finger flexion and extension [55] and in dynamic conditions [36], [64], [65], giving opportunity to work towards neural drive estimation with concurrent, dynamic actuation of the wrist and fingers flexing and extending. Additionally, we only observed postural effects on activation distribution of EMG. Dynamic motion may further affect recorded MUAPs, and studying captured MUAPs' properties across postures could further quantify MU decomposition's robustness.

V. CONCLUSION

In summary, we showed MU discharges accurately predicted individual isometric finger extension force with the forearm at three rotational postures spanning its range of motion. Overall, MU discharges outperformed conventional EMG-amplitude across postures in fingers with less isolated activation. Additionally, MU information decomposed in one posture sufficiently predicted force output across the entire range of motion. Further testing may offer more robust control input signals to neural-machine interfaces in dexterous functional tasks.

REFERENCES

- I. Pisotta, D. Perruchoud, and S. Ionta, "Hand-in-hand advances in biomedical engineering and sensorimotor restoration," *J. Neurosci. Methods*, vol. 246, pp. 22–29, May 2015, doi: 10.1016/j.jneumeth.2015.03.003.
- [2] T. J. Sullivan et al., "A brain-machine interface using dry-contact, low-noise EEG sensors," in Proc. IEEE Int. Symp. Circuits Syst., 2008, pp. 1986–1989, doi: 10.1109/ISCAS.2008.4541835.

566

567

568

569

570

571

572

573

574

575

576

577

578

579

580

581

582

583

584

585

586

587

588

589

590

591

592

593

594

595

596

597

598

599

600

601

602

603

604

605

606

607

608

609

610

611

612

613 614

615

616

617

618

619

620

621

622 623

624

625

626

627

628

629

630

631

632

633

634

635

636

637

638

639

640

- [3] T. Milekovic *et al.*, "An online brain-machine interface using decoding of movement direction from the human electrocorticogram," J. Neural Eng., vol. 9, no. 4, Aug. 2012, Art. no. 046003, doi: 10.1088/1741-2560/9/4/046003.
- [4] E. M. Maynard, C. T. Nordhausen, and R. A. Normann, "The utah intracortical electrode array: A recording structure for potential braincomputer interfaces," *Electroencephalogr. Clin. Neurophysiol.*, vol. 102, no. 3, pp. 228–239, Mar. 1997, doi: 10.1016/S0013-4694(96)95176-0.
- [5] J. del Valle and X. Navarro, "Interfaces with the peripheral nerve for the control of neuroprostheses," *Int. Rev. Neurobiol.*, vol. 109, 2013, pp. 63–83.
- [6] M. R. Ahsan, M. Ibrahimy, and O. O. Khalifa, "EMG signal classification for human computer interaction a review," *Eur. J. Sci. Res.*, vol. 33, no. 3, pp. 480–501, 2009. [Online]. Available: http://www.eurojournals. com/ejsr.htm
- [7] S. J. Day and M. Hulliger, "Experimental simulation of cat electromyogram: Evidence for algebraic summation of motor-unit action-potential trains," *J. Neurophysiol.*, vol. 86, no. 5, pp. 2144–2158, 2001, doi: 10.1152/jn.2001.86.5.2144.
- [8] J. Duchateau and R. M. Enoka, "Human motor unit recordings: Origins and insight into the integrated motor system," *Brain Res.*, vol. 1409, pp. 42–61, 2011, doi: 10.1016/j.brainres.2011.06.011.
- [9] P. A. Parker and R. N. Scott, "Myoelectric control of prostheses," *Crit. Rev. Biomed. Eng.*, vol. 13, no. 4, pp. 283–310, Jan. 1986. Accessed: Oct. 16, 2020. [Online]. Available: https://europepmc.org/article/med/3512166
- [10] E. Scheme and K. Englehart, "Electromyogram pattern recognition for control of powered upper-limb prostheses: State of the art and challenges for clinical use," *J. Rehabil. Res. Develop.*, vol. 48, no. 6, pp. 643–660, 2011, doi: 10.1682/JRRD.2010.09.0177.
- [11] A. Ajiboye and R. F. Weir, "A heuristic fuzzy logic approach to EMG pattern recognition for multifunctional prosthesis control," *IEEE Trans. Neural Syst. Rehabil. Eng.*, vol. 13, no. 3, pp. 280–291, Sep. 2005, doi: 10.1109/TNSRE.2005.847357.
- [12] G. Li, A. E. Schultz, and T. A. Kuiken, "Quantifying pattern recognition-based myoelectric control of multifunctional transradial prostheses," *IEEE Trans. Neural Syst. Rehabil. Eng.*, vol. 18, no. 2, pp. 185–192, Apr. 2010, doi: 10.1109/TNSRE.2009.2039619.
- [13] S. Lee and G. N. Saridis, "The control of a prosthetic arm by EMG pattern recognition," *IEEE Trans. Autom. Control*, vol. 29, no. 4, pp. 290–302, Apr. 1984, doi: 10.1109/TAC.1984.1103521.
- [14] A. J. Younget al., "Classification of simultaneous movements using surface EMG pattern recognition," *IEEE Trans. Biomed. Eng.*, vol. 60, no. 5, pp. 1250–1258, May 2013, doi: 10.1109/TBME.2012.2232293.
- [15] C. L. Pulliam, J. M. Lambrecht, and R. F. Kirsch, "Electromyogram-based neural network control of transhumeral prostheses," *J. Rehabil. Res. Develop.*, vol. 48, no. 6, pp. 739–754, 2011, doi: 10.1682/JRRD.2010.12.0237.
- [16] F. Xu, Y. Zheng, and X. Hu, "Real-time finger force prediction via parallel convolutional neural networks: A preliminary study," in *Proc. Annu. Int. Conf. IEEE Eng. Med. Biol. Soc.*, Jul. 2020, pp. 3126–3129, doi: 10.1109/EMBC44109.2020.9175390.
- [17] J. M. Hahne *et al.*, "Simultaneous control of multiple functions of bionic hand prostheses: Performance and robustness in end users," *Sci. Robot.*, vol. 3, Jun. 2018, Art. no. 19, doi: 10.1126/scirobotics.aat3630.
- [18] D. L. Crouch and H. Huang, "Lumped-parameter electromyogram-driven musculoskeletal hand model: A potential platform for real-time prosthesis control," *J. Biomech.*, vol. 49, no. 16, pp. 3901–3907, 2016, doi: 10.1016/j.jbiomech.2016.10.035.
- [19] M. Sartori et al., "Robust simultaneous myoelectric control of multiple degrees of freedom in wrist-hand prostheses by real-time neuro-musculoskeletal modeling," J. Neural Eng., vol. 15, no. 6, Oct. 2018, Art. no. 066026, doi: 10.1088/1741-2552/aae26b.
- [20] C. J. De Luca et al., "Decomposition of surface EMG signals," J. Neurophysiol., vol. 96, no. 3, pp. 1646–1657, 2006, doi: 10.1152/jn.00009.2006.
- [21] F. Negro et al., "Multi-channel intramuscular and surface EMG decomposition by convolutive blind source separation," J. Neural Eng., vol. 13, no. 2, Apr. 2016, Art. no. 026027, doi: 10.1088/1741-2560/13/2/026027.
- [22] H. Nakamura et al., "The application of independent component analysis to the multi-channel surface electromyographic signals for separation of motor unit action potential trains: Part I—Measuring techniques," J. Electromyogr. Kinesiol., vol. 14, no. 4, pp. 423–432, Aug. 2004, doi: 10.1016/j.jelekin.2004.01.004.
- [23] M. Chen and P. Zhou, "A novel framework based on FastICA for high density surface EMG decomposition," *IEEE Trans. Neural Syst. Rehabil. Eng.*, vol. 24, no. 1, pp. 117–127, Jan. 2016, doi: 10.1109/TNSRE.2015.2412038.

[24] M. Chen et al., "Automatic implementation of progressive FastICA peel-off for high density surface EMG decomposition," IEEE Trans. Neural Syst. Rehabil. Eng., vol. 26, no. 1, pp. 144–152, Jan. 2018, doi: 10.1109/TNSRE.2017.2759664. 641

642

643

644

645

646

647

648

649

650

651

652

653

654

656

657

658

659

660

661

662

663

664

666

667

668

669

670

671

672

673

674

675

676

677

678

679

680

681

682

683

684

685

686

687

688

689

690

691

692

693

694

695

696

697

699

700

701

702

703

704

705

707

708

709

710

711

712

713

714

715

706 **Q2**

- [25] Y. Zheng and X. Hu, "Concurrent prediction of finger forces based on source separation and classification of neuron discharge information," *Int. J. Neural Syst.*, vol. 31, no. 6, Jun. 2021, Art. no. 2150010, doi: 10.1142/S0129065721500106.
- [26] C. J. De Luca and Z. Erim, "Common drive of motor units in regulation of muscle force," *Trends Neurosci.*, vol. 17, no. 7, pp. 299–305, 1994, doi: 10.1016/0166-2236(94)90064-7.
- [27] J. G. Kreifeldt, "Signal versus noise characteristics of filtered emg used as a control source," *IEEE Trans. Biomed. Eng.*, vol. BME-18, no. 1, pp. 16–22, Jan. 1971, doi: 10.1109/TBME.1971.4502784.
- [28] C. J. De Luca *et al.*, "Filtering the surface EMG signal: Movement artifact and baseline noise contamination," *J. Biomech.*, vol. 43, no. 8, pp. 1573–1579, May 2010, doi: 10.1016/j.jbiomech.2010.01.027.
- [29] L. Mesin, "Crosstalk in surface electromyogram: Literature review and some insights," *Phys. Eng. Sci. Med.*, vol. 43, no. 2, pp. 481–492, Jun. 2020, doi: 10.1007/s13246-020-00868-1.
- [30] A. J. Young, L. J. Hargrove, and T. A. Kuiken, "The effects of electrode size and orientation on the sensitivity of myoelectric pattern recognition systems to electrode shift," *IEEE Trans. Biomed. Eng.*, vol. 58, no. 9, pp. 2537–2544, Sep. 2011, doi: 10.1109/TBME.2011.2159216.
- [31] J. Liu *et al.*, "Quantification and solutions of arm movements effect on sEMG pattern recognition," *Biomed. Signal Process. Control*, vol. 13, pp. 189–197, 2014, doi: 10.1016/j.bspc.2014.05.001.
- [32] C. A. Buneo, J. F. Soechting, and M. Flanders, "Postural dependence of muscle actions: Implications for neural control," *J. Neurosci.*, vol. 17, no. 6, pp. 2128–2142, Mar. 1997, doi: 10.1523/jneurosci.17-06-02128.1997.
- [33] J. Mogk and P. Keir, "The effects of posture on forearm muscle loading during gripping," *Ergonomics*, vol. 46, no. 9, pp. 956–975, 2003, doi: 10.1080/0014013031000107595.
- [34] A. Hyvarinen, "Fast and robust fixed-point algorithms for independent component analysis," *IEEE Trans. Neural Netw.*, vol. 10, no. 3, pp. 626–634, May 1999, doi: 10.1109/72.761722.
- [35] Y. Zheng and X. Hu, "Interference removal from electromyography based on independent component analysis," *IEEE Trans. Neural Syst. Rehabil. Eng.*, vol. 27, no. 5, pp. 887–894, 2019, doi: 10.1109/TNSRE.2019.2910387.
- [36] T. Kapelner et al., "Predicting wrist kinematics from motor unit discharge timings for the control of active prostheses," J. Neuroeng. Rehabil., vol. 16, no. 1, 2019, Art. no. 47, doi: 10.1186/s12984-019-0516-x.
- [37] X. Hu *et al.*, "Extracting extensor digitorum communis activation patterns using high-density surface electromyography," *Front. Physiol.*, vol. no. 6, Oct. 2015, Art. no. 279, doi: 10.3389/fphys.2015.00279.
- [38] C. Dai, Y. Zheng, and X. Hu, "Estimation of muscle force based on neural drive in a hemispheric stroke survivor," *Front. Neurol.*, vol. 9, 2018, Art. no. 187, doi: 10.3389/fneur.2018.00187.
- [39] C. Dai and X. Hu, "Finger joint angle estimation based on motoneuron discharge activities," *IEEE J. Biomed. Health Inform.*, vol. 24, no. 3, pp. 760–767, Mar. 2020, doi: 10.1109/JBHI.2019.2926307.
- [40] C. Dai and X. Hu, "Independent component analysis based algorithms for high-density electromyogram decomposition: Systematic evaluation through simulation," *Comput. Biol. Med.*, vol. 109, pp. 171–181, 2019, doi: 10.1016/j.compbiomed.2019.04.033.
- [41] D. Falla and D. Farina, "Periodic increases in force during sustained contraction reduce fatigue and facilitate spatial redistribution of trapezius muscle activity," *Exp. Brain Res.*, vol. 182, no. 1, pp. 99–107, 2007, doi: 10.1007/s00221-007-0974-4.
- [42] S. S. Shapiro and M. B. Wilk, "An analysis of variance test for normality (complete samples)†," *Biometrika*, vol. 52, no. 3–4, pp. 591–611, Dec. 1965, doi: 10.1093/biomet/52.3-4.591.
- [43] T. W. Parks and C. S. Burrus, *Digital Filter Design*. Hoboken, NJ, USA: Wiley, 1987.
- [44] Y. Zheng and X. Hu, "Real-time isometric finger extension force estimation based on motor unit discharge information," *J. Neural Eng.*, vol. 16, no. 6, 2019, Art. no. 66006, doi: 10.1088/1741-2552/ab2c55.
- [45] Y. Zheng and X. Hu, "Dexterous force estimation during finger flexion and extension using motor unit discharge information," in *Proc. 42nd Annu. Int. Conf. IEEE Eng. Med. Biol. Soc.*, July 2020, vol. 2020-Jul., pp. 3130–3133, doi: 10.1109/EMBC44109.2020.9175236.
- [46] R. E. Kalman, "A new approach to linear filtering and prediction problems," *Trans. ASME-J. Basic Eng.*, vol. 82, pp. 35–45, 1960.

753

754

755

756

757

758

759

760

761

762

763

764

765

767

768

769

770

771

772

773

774

775

776

777

778

779

780

781

782

717 [47] D. Farina, F. Negro, and J. L. Dideriksen, "The effective neural drive to muscles is the common synaptic input to motor neurons," *J. Physiol.*, vol. 592, no. 16, pp. 3427–3441, 2014, doi: 10.1113/jphys-iol.2014.273581.

721

722

723

724

725

726

727

728

729

730

731

732

733

734

735

736

737

738

739

740

741

742

743

744

745

746

747

- [48] J. W. Mauchly, "Significance test for sphericity of a normal n-Variate distribution," *Ann. Math. Statist.*, vol. 11, no. 2, pp. 204–209, Nov. 1940. [Online]. Available: http://www.jstor.org/stable/2235878
- [49] N. van Beek et al., "Activity patterns of extrinsic finger flexors and extensors during movements of instructed and non-instructed fingers," J. Electromyogr. Kinesiol., vol. 38, pp. 187–196, Feb. 2018, doi: 10.1016/j.jelekin.2017.02.006.
- [50] C. Dai and X. Hu, "Extracting and classifying spatial muscle activation patterns in forearm flexor muscles using high-density electromyogram recordings," *Int. J. Neural Syst.*, vol. 29, no. 1, Art. no. 1850025, Feb. 2019, doi: 10.1142/S0129065718500259.
- [51] A. W. English, S. L. Wolf, and R. L. Segal, "Compartmentalization of muscles and their motor nuclei: The partitioning hypothesis," *Phys. Ther.*, vol. 73, no. 12, pp. 857–867, 1993, doi: 10.1093/ptj/73.12.857.
- [52] A. T. Liu *et al.*, "Architectural properties of the neuromuscular compartments in selected forearm skeletal muscles," *J. Anatomy*, vol. 225, no. 1, pp. 12–18, 2014, doi: 10.1111/joa.12193.
- [53] J. N. A. L. Leijnse et al., "Assessment of individual finger muscle activity in the extensor digitorum communis by surface EMG," J. Neurophysiol., vol. 100, no. 6, pp. 3225–3235, Dec. 2008, doi: 10.1152/jn.90570.2008.
- [54] W. S. Yu, H. Van Duinen, and S. C. Gandevia, "Limits to the control of the human thumb and fingers in flexion and extension," *J. Neurophysiol.*, vol. 103, no. 1, pp. 278–289, Jan. 2010, doi: 10.1152/jn.00797.2009.
- [55] Y. Zheng and X. Hu, "Concurrent estimation of finger flexion and extension forces using motoneuron discharge information," *IEEE Trans. Biomed. Eng.*, vol. 68, no. 5, pp. 1638–1645, May 2021, doi: 10.1109/TBME.2021.3056930.
- [56] J. N. A. L. Leijnse *et al.*, "Anatomic basis for individuated surface EMG and homogeneous electrostimulation with neuroprostheses of the extensor digitorum communis," *J. Neurophysiol.*, vol. 100, no. 1, pp. 64–75,
 Jul. 2008, doi: 10.1152/jn.00706.2007.

- [57] V. M. Zatsiorsky, Z. M. Li, and M. L. Latash, "Coordinated force production in multi-finger tasks: Finger interaction and neural network modeling," *Biol. Cybern.*, vol. 79, no. 2, pp. 139–150, 1998, doi: 10.1007/s004220050466.
- [58] V. M. Zatsiorsky, Z.-M. Li, and M. L. Latash, "Enslaving effects in multi-finger force production," *Exp. Brain Res.*, vol. 131, no. 2, pp. 187–195, 2000, doi: 10.1007/s002219900261.
- [59] S. Bodine-Fowler et al., "Spatial distribution of muscle fibers within the territory of a motor unit," Muscle Nerve, vol. 13, no. 12, pp. 1133–1145, 1990, doi: 10.1002/mus.880131208.
- [60] A. Schmied, C. Ivarsson, and E. E. Fetz, "Short-term synchronization of motor units in human extensor digitorum communis muscle: Relation to contractile properties and voluntary control," *Exp. Brain Res.*, vol. 97, no. 1, pp. 159–172, Dec. 1993, doi: 10.1007/BF00228826.
- [61] C. Dai *et al.*, "Origins of common neural inputs to different compartments of the extensor digitorum communis muscle," *Sci. Rep.*, vol. 7, 2017, Art. no. 13960, doi: 10.1038/s41598-017-14555-x.
- [62] C. E. Lang and M. H. Schieber, "Human finger independence: Limitations due to passive mechanical coupling versus active neuromuscular control," *J. Neurophysiol.*, vol. 92, no. 5, pp. 2802–2810, 2004, doi: 10.1152/jn.00480.2004.
- [63] H. van Duinen, W. S. Yu, and S. C. Gandevia, "Limited ability to extend the digits of the human hand independently with extensor digitorum," *J. Physiol.*, vol. 587, no. Pt 20, pp. 4799–4810, 2009, doi: 10.1113/jphys-iol.2009.177964.
- [64] C. J. De Luca et al., "Decomposition of surface EMG signals from cyclic dynamic contractions," J. Neurophysiol., vol. 113, no. 6, pp. 1941–1951, 2015, doi: 10.1152/jn.00555.2014.
- [65] M. D. Twardowski et al., "Motor unit drive: A neural interface for real-time upper limb prosthetic control," J. Neural Eng., vol. 16, no. 1, Feb. 2019, Art. no. 016012, doi: 10.1088/1741-2552/aaeb0f.